

# Locality Preserving Refinement for Shape Matching with Functional Maps

Yifan Xia, Yifan Lu, Yuan Gao\*, and Jiayi Ma\*

Electronic Information School, Wuhan University, Wuhan 430072, China  
xiayifan@whu.edu.cn, lyf048@whu.edu.cn, ethan.y.gao@gmail.com, jyama2010@gmail.com

## Abstract

In this paper, we address the nonrigid shape matching with outliers by a novel and effective pointwise map refinement method, termed *Locality Preserving Refinement*. For accurate pointwise conversion from a given functional map, our method formulates a two-step procedure. Firstly, starting with noisy point-to-point correspondences, we identify inliers by leveraging the neighborhood support, which yields a closed-form solution with linear complexity. After obtained the reliable correspondences of inliers, we refine the pointwise correspondences for outliers using local linear embedding, which operates in an adaptive spectral similarity space to further eliminate the ambiguities that are difficult to handle in the functional space. By refining pointwise correspondences with local consistency thus embedding geometric constraints into functional spaces, our method achieves considerable improvement in accuracy with linearithmic time and space cost. Extensive experiments on public benchmarks demonstrate the superiority of our method over the state-of-the-art methods. Our code is publicly available at <https://github.com/XiaYifan1999/LOPR>.

## Introduction

Recognizing the similarity and correspondences between two nonrigid shapes is a fundamental problem in computer vision and graphics (Van Kaick et al. 2011; Sahillioğlu 2020), such as shape analysis (Hartman et al. 2023), style transfer (Sumner and Popović 2004), pose estimation (Jiang et al. 2022), and texture mapping (Ezuz and Ben-Chen 2017). Unlike rigid alignment with easy parametric modeling, the complexity of nonrigid transformation and the existence of unknown outliers make such a problem intractable to be modeled.

Due to the approximately isometric nature of real-world deformations, estimating the near-isometric maps for nonrigid shape matching receives increasing research interests in the last decades (Sahillioğlu 2020). Among the numerous strategies for seeking the near-isometric maps (Deng et al. 2022), functional maps (Ovsjanikov et al. 2012) stands out as an exemplary technique due to its high efficiency. Observing the isometric invariance based on the Laplacian-Beltrami

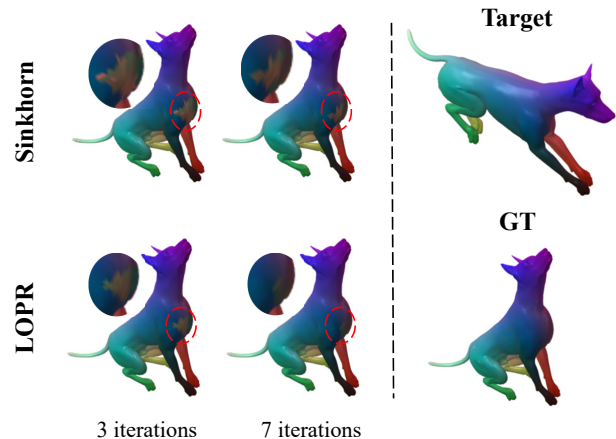


Figure 1: Qualitative examples employing color transfer, comparing our LOPR with representative state-of-the-art Sinkhorn (Pai et al. 2021) by integrating them into the iteration of MWP. Notably, our LOPR exhibits the capacity to recover more precise pointwise maps.

operator, functional map framework proposes the determination of a functional map operator that maps two spaces of square-integrable functions on respective shape, thereby efficiently recovering pointwise correspondences. This enables algebraic operations on shape maps such as map sum, and natural constraints become linear. For instance, local volume preserving maps can be associated with the orthogonality of functional map matrices, near isometries correspond to the commutativity of Laplacian operator, and conformal maps would preserve functional inner products. Interested readers are referred to the introductory course (Ovsjanikov et al. 2016) for details.

Following the functional map framework, many works are presented in recent years. BCICP (Ren et al. 2018) is proposed to promote orientation preservation. PFM (Rodolà et al. 2017) is devised for partial shape matching. Moreover, ZoomOut (Melzi et al. 2019), SmoothShells (Eisenberger, Lahner, and Cremers 2020), DiscreteOp (Ren et al. 2021), MWP (Hu et al. 2021), CFM (Donati et al. 2022), and EDEO (Magnet et al. 2022) are proposed to enhance the effectiveness of functional maps. The pointwise map recoveries of all these methods draw inspiration from ICP proposed by original work (Ovsjanikov et al. 2012), *i.e.*, an iter-

\*Corresponding author

ative refinement based on Nearest Neighbor (NN) searches between eigenfunction matrices. However, this strategy is subject to the absence of topological constraints from Euclidean space, thus hindering properties of pointwise correspondences such as continuity and smoothness. Therefore, a recurring problem of functional map framework lies in prohibiting precise alignment at fine scales.

Several works (Rodolà, Moeller, and Cremers 2015; Rodola, Möller, and Cremers 2017; Pai et al. 2021) have noted this ill-defined problem of pointwise conversion from a functional map. PMF (Vestner et al. 2017b) and Kernel-Matching (Vestner et al. 2017a) both utilize the kernel density estimation for correspondence recovery but suffer from high computational burden. Fast Sinkhorn Filters (Pai et al. 2021) combines the functional map representation with the matrix scaling schemes from computational optimal transport. Nevertheless, this method is limited to the spectral embedding alignment, leaving room for improvement in terms of accuracy and complexity. COMB (Roetzer et al. 2022) devises a scalable combinatorial solver but suffers from high computational burden. GCPD (Fan et al. 2022) generalizes the kernel techniques based on classic CPD (Myronenko and Song 2010) to achieve extrinsic alignment, however relies on functional map methods as initialization. In conclusion, pointwise map recovery, as a widely prevalent step in functional map framework, exhibits evident limitations while holding significant significance and broad value. Existing methods either suffer from inadequate precision (e.g., nearest neighbors) or incur significant time and memory cost (e.g., assignment solvers).

In order to release above limitations, we propose an efficient framework named *LOcality Preserving Refinement* (LOPR), which recovers more precise pointwise maps with explicit continuity and smoothness constraints. Given noisy pointwise maps have erroneous point-to-point correspondences as outliers, we firstly establish a mathematical model to differentiate between correct correspondences (inliers) and outliers. Observing local consistency during various deformations, we derive a closed-form solution with linear time and space complexity based on meshed neighborhood support to ensure continuity between points. Subsequently, we perform re-matching for the outliers using reliable mapping relations from the inliers. Specifically, to estimate a weight matrix based on Locally Linear Embedding (LLE), we construct neighborhoods from inliers for outliers in source shape. Then, in the target shape, we select appropriate corresponding points from the K-nearest neighbors in the spectral domain with the minimum reconstruction errors of LLE, thus avoiding the previous ambiguity of searching only the nearest neighbors in the spectral domain. Additionally, our hyperparameters can be selected adaptively, ensuring the applicability to diverse resolutions. Qualitative comparisons with the recent pointwise map recovery method Sinkhorn (Pai et al. 2021) are shown in Fig. 1.

In summary, the primary contributions are threefold:

- We propose a novel and effective framework for pointwise map recovery, which embeds topological constraints from Euclidean spaces into the functional space.

- Drawing on the local consistency within nonrigid deformations, we formulate a concise mathematical model that offers a closed-form solution with linear complexity and devise an outlier refinement strategy via LLE.
- We conduct extensive experiments on public datasets to compare our method against state-of-the-art methods, which demonstrate the superiority of our method.

## Functional Maps Revisited

Given a shape modeled as a smooth compact two-dimensional manifold  $\mathcal{M}$  with area element  $d\mu$  embedded into  $\mathbb{R}^3$ , the space of square-integrable functions on the manifold  $\mathcal{M}$  is denoted by  $\mathcal{L}^2(\mathcal{M}) = \{f : \mathcal{M} \rightarrow \mathbb{R}, \int_{\mathcal{M}} f(x)^2 d\mu < \infty\}$ . With the symmetric Laplace-Beltrami operator  $\Delta_{\mathcal{M}}$  providing Fourier analysis to manifold  $\mathcal{M}$ , there exists an eigen-decomposition  $\Delta_{\mathcal{M}}\phi_i = \lambda_i\phi_i$  for  $i \geq 1$  with eigenfunctions  $\{\phi_i\}_{i \geq 1}$  as an orthonormal basis and eigenvalues  $0 = \lambda_1 < \lambda_2 \leq \dots$  of  $\mathcal{L}^2(\mathcal{M})$ . In this case, any function  $f \in \mathcal{L}^2(\mathcal{M})$  can be represented as  $f(x) = \sum_{i \geq 1} \langle f, \phi_i \rangle_{\mathcal{M}} \phi_i(x)$ , where  $\langle \cdot \rangle_{\mathcal{M}}$  denotes the inner product on the manifold  $\mathcal{M}$ .

## Functional Correspondence

As proposed by the original work (Ovsjanikov et al. 2012), the shape correspondences can be obtained by transferring functions between manifolds. Given a pointwise map  $T: \mathcal{M} \rightarrow \mathcal{N}$  and a functional map  $T_F: \mathcal{L}^2(\mathcal{M}) \rightarrow \mathcal{L}^2(\mathcal{N})$  from a manifold  $\mathcal{M}$  to another manifold  $\mathcal{N}$ , the image of any function  $f \in \mathcal{L}^2(\mathcal{M})$  is defined as  $T_F(f) = f \circ T^{-1}$ . Considering two orthonormal bases  $\{\phi_i^{\mathcal{M}}\}_{i \geq 0}$  and  $\{\phi_j^{\mathcal{N}}\}_{j \geq 0}$  of  $\mathcal{L}^2(\mathcal{M})$  and  $\mathcal{L}^2(\mathcal{N})$ , respectively, the functional image is represented as:

$$T_F(f) = \sum_j \sum_i \langle f, \phi_i^{\mathcal{M}} \rangle_{\mathcal{M}} \underbrace{\langle T_F(\phi_i^{\mathcal{M}}), \phi_j^{\mathcal{N}} \rangle_{\mathcal{N}}}_{c_{ji}} \phi_j^{\mathcal{N}}. \quad (1)$$

We denote the matrix  $\mathbf{C} = [c_{ji}] \in \mathbb{R}^{k \times k}$ , which maps the first  $k$  eigenfunctions to efficiently approximate smooth correspondence. The unknown matrix  $\mathbf{C}$  encodes the functional map  $T_F$ , which can be derived by linear constraints such as descriptor and segment preservation together with the operator commutativity (Ovsjanikov et al. 2012).

## Pointwise Map Recovery

Given a functional map  $T_F$ , the pointwise map  $T$  between two discrete shapes can be reconstructed (Ovsjanikov et al. 2012). Specifically, for any point  $x$  on  $\mathcal{M}$ , its corresponding point  $T(x)$  in  $\mathcal{N}$  is denoted as  $T(x) = \arg \max_y T_F(\delta_x)(y)$ , where  $\delta_x$  is the delta-function at point  $x$  on the shape  $\mathcal{M}$ . As  $\langle \delta_x, \phi_i \rangle = \phi_i(x)$ , if let the matrices  $\Phi_{\mathcal{M}} \in \mathbb{R}^{m \times k}$  and  $\Phi_{\mathcal{N}} \in \mathbb{R}^{n \times k}$  respectively denote the first  $k$  Laplace-Beltrami eigenfunctions of  $\mathcal{M}$  and  $\mathcal{N}$ , where each column corresponds to an eigenfunction and each row to a point, each row vector of  $\mathbf{C}(\Phi_{\mathcal{M}})^{\top}$  represents transferred Fourier coefficients of a point on  $\mathcal{M}$  and has high similarity to a row vector of  $\Phi_{\mathcal{N}}^{\top}$  corresponding its matching point on  $\mathcal{N}$ . By Plancherel's theorem (Penney 1975), the distances between

coefficient vectors of functions can be computed by  $L^2$  differences. Thus, the pointwise map  $T$  can be recovered by minimizing the following function:

$$\min_T \sum_{i=1}^m \left\| \mathbf{C}(\Phi_{\mathcal{M}}(i))^\top - (\Phi_{\mathcal{N}}(T(i)))^\top \right\|_2, \quad (2)$$

where  $\Phi_{\mathcal{M}}(i)$  represents the  $i$ -th row of matrix  $\Phi_{\mathcal{M}}$  and  $\Phi_{\mathcal{N}}(T(i))$  corresponds to the mapping point of point  $i$  on  $\mathcal{N}$ . Eq. (2) can be solved by nearest neighbor search via KD tree. In this way, the high-dimensional pointwise maps  $T$  can be recovered from the functional spaces, though may suffer from limited accuracy and continuity.

## Methodology

This section describes our LOPR for pointwise map recovery in functional maps, where an effective framework based on local consistency is proposed to refine noisy point-to-point correspondences towards a better performance. Given that pointwise maps incorporate correct correspondences (inliers) and incorrect ones (outliers), our proposed framework involves two steps: (i) distinguish inliers and outliers from noisy pointwise maps; (ii) refine point correspondences of outliers based on the reliable mapping of inliers.

### Distinguish Inliers via Neighborhood Consensus

Given that  $\mathcal{X} = \{\mathbf{x}_i\}_{i=1}^m$  and  $\mathcal{Y} = \{\mathbf{y}_i\}_{i=1}^n$  are two vector sets of vertex spatial coordinates on two discrete manifolds  $\mathcal{M}$  and  $\mathcal{N}$ , respectively, denoting  $T_0 \in \mathbb{R}^m$  an initial pointwise map that maps each point from  $\mathcal{M}$  to a point of  $\mathcal{N}$ , our first goal is to distinguish the inliers from a noisy point correspondence set  $\{\mathbf{x}_i, \mathbf{y}_{T_0(i)}\}_{i=1}^m$ .

**Ideal Isometric Formulation** Denoting  $\mathcal{I}$  an unknown inlier set,  $C$  as a cost function, we have the following objective to find the inliers in the isometric transformation case:

$$\mathcal{I}^* = \arg \min_{\mathcal{I}} C(\mathcal{I}; \mathcal{X}, \mathcal{Y}, T_0, \lambda). \quad (3)$$

Since the distance between two arbitrary points in  $\mathcal{M}$  preserves the same as that of their corresponding points in  $\mathcal{N}$ , the cost function  $C$  can be defined as

$$C(\mathcal{I}; \mathcal{X}, \mathcal{Y}, T_0, \lambda) = \sum_{i \in \mathcal{I}} \sum_{j \in \mathcal{I}} (d(\mathbf{x}_i, \mathbf{x}_j) - d(\mathbf{y}_{T_0(i)}, \mathbf{y}_{T_0(j)}))^2 + \lambda(|T_0| - |\mathcal{I}|), \quad (4)$$

where  $d$  is the geodesic distance, and  $|T_0| = m$ . The first term of Eq. (4) restricts the variance of geodesic distances between any two point pairs, and the second term discourages the outliers with a balance parameter  $\lambda > 0$ . Ideally, this cost function should be minimized to zero.

**General Shape Matching** Real applications generally require the acquisition and analysis about nonrigidly deformable objects. Though complex nonrigid deformations produces non-isometric maps, the topology of local structure is consistent. In discrete setting, the point distribution

in a local region is preserved even after a severe deformation. Thus, we have a more general form of Eq. (4):

$$C(\mathcal{I}; \mathcal{X}, \mathcal{Y}, T_0, \lambda) = \sum_{i \in \mathcal{I}} \frac{1}{|N_{\mathbf{x}_i}| + |N_{\mathbf{y}_{T_0(i)}}|} \left( \sum_{j|\mathbf{x}_j \in N_{\mathbf{x}_i}} (d(\mathbf{x}_i, \mathbf{x}_j) - d(\mathbf{y}_{T_0(i)}, \mathbf{y}_{T_0(j)}))^2 + \sum_{j|\mathbf{y}_{T_0(j)} \in N_{\mathbf{y}_{T_0(i)}}} (d(\mathbf{x}_i, \mathbf{x}_j) - d(\mathbf{y}_{T_0(i)}, \mathbf{y}_{T_0(j)}))^2 \right) + \lambda(|T_0| - |\mathcal{I}|), \quad (5)$$

where  $N_{\mathbf{x}}$  denotes the neighborhood of vertex  $\mathbf{x}$ , which is  $\mathbf{x}$ 's adjacent points under triangular meshing. Due to the severe deformations, we only assume the distance preserves in a local (neighboring/adjacent) region, therefore, the distance  $d$  in Eq. (5) is:

$$d(\mathbf{x}_i, \mathbf{x}_j) = \begin{cases} 0, & \mathbf{x}_j \in N_{\mathbf{x}_i} \\ 1, & \mathbf{x}_j \notin N_{\mathbf{x}_i} \end{cases}, \quad (6)$$

and we also have a similar definition for  $d(\mathbf{y}_i, \mathbf{y}_j)$ .

Let a binary vector  $\mathbf{p}$  be the correctness of correspondences, where  $p_i = 1$  represents an inlier ( $\mathbf{x}_i, \mathbf{y}_{T_0(i)}$ ), otherwise an outlier. Substituting Eq. (6) into the cost function Eq. (5), we have

$$C(\mathbf{p}; \mathcal{X}, \mathcal{Y}, T_0, \lambda) = \sum_{i=1}^m \frac{p_i}{|N_{\mathbf{x}_i}| + |N_{\mathbf{y}_{T_0(i)}}|} \left( \sum_{j|\mathbf{x}_j \in N_{\mathbf{x}_i}} d(\mathbf{y}_{T_0(i)}, \mathbf{y}_{T_0(j)}) + \sum_{j|\mathbf{y}_{T_0(j)} \in N_{\mathbf{y}_{T_0(i)}}} d(\mathbf{x}_i, \mathbf{x}_j) \right) + \lambda(m - \sum_{i=1}^m p_i). \quad (7)$$

In this case, the topological constraints based on locality consistency are invariant to translation, rotation, and scale, facilitating the robustness for various deformations.

**Optimization** To minimize the cost function Eq. (7), we reformulate it by merging the terms related to  $p_i$  as:

$$C(\mathbf{p}; \mathcal{X}, \mathcal{Y}, T_0, \lambda) = \sum_{i=1}^m p_i(c_i - \lambda) + \lambda m, \quad (8)$$

where  $c_i$  is defined as the disparity score:

$$c_i = 1 - \frac{2n_i}{|N_{\mathbf{x}_i}| + |N_{\mathbf{y}_{T_0(i)}}|}, \quad (9)$$

and  $n_i = \text{count}(j|\mathbf{x}_j \in N_{\mathbf{x}_i}, \mathbf{y}_{T_0(j)} \in N_{\mathbf{y}_{T_0(i)}})$  is the number of shared elements in two neighborhoods. We note that  $c_i$  is approximate to 0 if  $(\mathbf{x}_i, \mathbf{y}_{T_0(i)})$  is an ideally correct correspondence.

Since a surface usually consists of a vary large number of vertices (*e.g.*, ten thousands), it is necessary to consider not only a single neighborhood. Thus to better describe the structure of local region, we extend the disparity score  $c_i$  into

$$\tilde{c}_i = \frac{c_i + \sum_{j|\mathbf{x}_j \in N_{\mathbf{x}_i}} c_j}{1 + |N_{\mathbf{x}_i}|}, \quad (10)$$

and the cost function is updated as

$$C(\mathbf{p}; \mathcal{X}, \mathcal{Y}, T_0, \lambda) = \sum_{i=1}^m p_i(\tilde{c}_i - \lambda) + \lambda|T_0|. \quad (11)$$

Eq. (11) shows that any correspondence with  $\tilde{c}_i > \lambda$  produces a positive term to increase the cost function, while that with  $\tilde{c}_i < \lambda$  leads to a negative term thus decreasing the objective.  $\lambda$  is a balance factor that determines the trade-off between two terms in Eq. (4), *i.e.*, the higher value of  $\lambda$ , the smaller and more reliable the set  $\mathcal{I}$  is.

Apparently the consensus score  $\{\tilde{c}_i\}_{i=1}^m$  can be computed in advance. Given triangular meshing and mapping  $T_0$  of two manifolds, therefore, the optimal  $\mathbf{p}$  minimizing Eq. (11) can be obtained by:

$$p_i = \begin{cases} 1, & \tilde{c}_i \geq \lambda, \\ 0, & \tilde{c}_i < \lambda, \end{cases} \quad i = 1, \dots, m. \quad (12)$$

Hence, the optimal inlier set  $\mathcal{I}^*$  is:

$$\mathcal{I}^* = \{i | p_i = 1, i = 1, \dots, m\}, \quad (13)$$

which is a reliable estimation not only satisfying local consistency, but also possessing well continuity due to the constraint of adjacent relations.

### Correspondence Refinement via LLE

An reliable inlier set  $\mathcal{I}$  can be used to refine the correspondences of outliers. To this end, we propose a local geometric constraint based on Locally Linear Embedding (LLE) (Roweis and Saul 2000). Exploiting the local consensus prior, LLE embeds the topology of a local region into a low-dimensional manifold, which learns a better distance metric with strong stability.

Specifically, we divide the vertex set  $\mathcal{X}$  into two parts:  $\mathcal{X}_{\mathcal{I}}$  indicates inliers with correct correspondences, and  $\mathcal{X}_{\mathcal{O}}$  denotes the outlier with mismatches. We also have similar  $\mathcal{Y}_{\mathcal{I}}$  and  $\mathcal{Y}_{\mathcal{O}}$  for  $\mathcal{Y}$ . Next, we show how to choose a corresponding vertex from  $\mathcal{Y}_{\mathcal{O}}$  for each point in  $\mathcal{X}_{\mathcal{O}}$  based on reliable maps  $(\mathcal{X}_{\mathcal{I}}, \mathcal{Y}_{\mathcal{I}})$ , which introduces geometric constraints in Euclidean space.

Firstly, for each point  $\mathbf{x}_i^{\mathcal{O}}$  of  $\mathcal{X}_{\mathcal{O}}$ , we search its  $K_1$  nearest neighbors from  $\mathcal{X}_{\mathcal{I}}$  with the  $L_2$  distance of their coordinates on manifold  $\mathcal{M}$ , obtaining a neighborhood set  $N_{\mathbf{x}_i^{\mathcal{O}}}^{K_1}$ :

$$N_{\mathbf{x}_i^{\mathcal{O}}}^{K_1} = K_1\text{-NNsearch}(\mathbf{x}_i^{\mathcal{O}}, \mathcal{X}_{\mathcal{I}}), \quad (14)$$

In this step,  $n_{\mathcal{O}}$  neighborhood sets will be generated, where  $n_{\mathcal{O}} = |\mathcal{X}_{\mathcal{O}}|$  is the number of points in  $\mathcal{X}_{\mathcal{O}}$ .

Secondly, to derive a weight matrix  $\mathbf{W} \in \mathbb{R}^{n_{\mathcal{O}} \times K_1}$ , we minimize the reconstruction errors measured by the following cost function:

$$\mathcal{E}(\mathbf{W}) = \sum_{i=1}^{n_{\mathcal{O}}} \left\| \mathbf{x}_i^{\mathcal{O}} - \sum_{j=1}^{K_1} \mathbf{W}_{ij} \mathbf{x}_{i,j} \right\|^2, \text{ s.t. } \forall i, \sum_{j=1}^{K_1} \mathbf{W}_{ij} = 1, \quad (15)$$

where  $\forall i, \mathbf{x}_{i,j} \in N_{\mathbf{x}_i^{\mathcal{O}}}^{K_1}, j = 1, \dots, K_1$ , and the topology of vertex distribution is preserved in the weight matrix  $\mathbf{W}$  via

---

### Algorithm 1: Locality Preserving Refinement for Pointwise Map Recovery

---

**Input:** A pair of discrete manifolds  $\mathcal{M}$  and  $\mathcal{N}$  with bases  $\Phi_{\mathcal{M}}$  and  $\Phi_{\mathcal{N}}$  and a functional map  $\mathbf{C}$

**Parameter:**  $\lambda$

**Output:** pointwise map  $T$

- 1: Obtain  $T_0$  by selecting nearest neighbors by Eq. (2);
  - 2: Calculate disparity scores  $\{c_i\}_{i=1}^m$  by Eq. (10);
  - 3: Determine optimal inlier set  $\mathcal{I}^*$  by Eq. (13);
  - 4: Construct neighborhoods  $\{N_{\mathbf{x}_i^{\mathcal{O}}}^{K_1}\}_{i=1}^{n_{\mathcal{O}}}$  by Eq. (14);
  - 5: Compute matrix  $\mathbf{W}$  by minimizing Eq. (15);
  - 6: Obtain outlier map  $T_{\mathcal{O}}$  by Eqs. (16) and (17);
  - 7: Obtain  $T$  by combining  $T_{\mathcal{O}}$  and  $T_{\mathcal{I}}$  from  $\mathcal{I}^*$ ;
- 

the neighboring point relationship. We can efficiently solve Eq. (15) for  $\mathbf{W}_{ij}$  by the least squares.

Thirdly, we seek the corresponding vertex  $\mathbf{y}_{T_{\mathcal{O}}(i)}^{\mathcal{O}}$  from  $\mathcal{Y}_{\mathcal{O}}$  to  $\mathbf{x}_i^{\mathcal{O}}$  from  $\mathcal{X}_{\mathcal{O}}$ , so as to obtain the pointwise map  $T_{\mathcal{O}}$  for outliers. We solve this in an embedded manifold representation using the spectral similarity. Specifically, we obtain  $K_1$  corresponding points  $T_{\mathcal{I}}(N_{\mathbf{x}_i^{\mathcal{O}}}^{K_1})$  of neighborhood  $N_{\mathbf{x}_i^{\mathcal{O}}}^{K_1}$  by pointwise map  $T_{\mathcal{I}}$ . Then, we find the  $K_2$  nearest neighbors between the column vectors of  $\mathbf{C}(\Phi_{\mathcal{M}}^{\mathcal{O}})^{\top}$  and  $(\Phi_{\mathcal{N}}^{\mathcal{O}})^{\top}$  as the spectral neighborhoods, where  $\Phi_{\mathcal{M}}^{\mathcal{O}}/\Phi_{\mathcal{N}}^{\mathcal{O}} \in \mathbb{R}^{n_{\mathcal{O}} \times k}$  is the matrix consisting of the row vectors of  $\Phi_{\mathcal{M}}/\Phi_{\mathcal{N}}$  corresponding to outliers  $\mathcal{X}_{\mathcal{O}}/\mathcal{Y}_{\mathcal{O}}$ , respectively. Next, the correspondence  $\mathbf{y}_{T_{\mathcal{O}}(i)}^{\mathcal{O}}$  of vertex  $\mathbf{x}_i^{\mathcal{O}}$  can be chosen as the vertex with minimal reconstruction error from the spectral neighborhood  $\mathcal{N}_{\mathbf{C}(\Phi_{\mathcal{M}}^{\mathcal{O}}(i))^{\top}}^{K_2}$ :

$$T_{\mathcal{O}}(i) = \arg \min_{j | \Phi_{\mathcal{N}}(j) \in \mathcal{N}_{\mathbf{C}(\Phi_{\mathcal{M}}^{\mathcal{O}}(i))^{\top}}^{K_2}} \left\| \mathbf{y}_j - \sum_{k=1}^{K_1} \mathbf{W}_{ik} \mathbf{y}_{i,k} \right\|^2, \quad (16)$$

where the spectral neighborhood

$$\mathcal{N}_{\mathbf{C}(\Phi_{\mathcal{M}}^{\mathcal{O}}(i))^{\top}}^{K_2} = K_2\text{-NNsearch}(\mathbf{C}(\Phi_{\mathcal{M}}^{\mathcal{O}}(i))^{\top}, (\Phi_{\mathcal{N}}^{\mathcal{O}})^{\top}), \quad (17)$$

and  $\forall i, \mathbf{x}_i^{\mathcal{O}} \in \mathcal{X}_{\mathcal{O}}, \mathbf{y}_{i,k} \in T_{\mathcal{I}}(N_{\mathbf{x}_i^{\mathcal{O}}}^{K_1}), k = 1, \dots, K_1$ . Finally, the pointwise maps  $T_{\mathcal{I}}$  for inliers and  $T_{\mathcal{O}}$  derived from Eq. (16) form a full pointwise map  $T$ . The overall algorithm flow is described in Algorithm 1.

Spectral ambiguity is the main issue that degrades the pointwise map recovery, which occurs when two points are not correct correspondence but with the highest similarity in Fourier coefficients. This happens when those two points are intrinsically symmetric, such as the left and right elbows of a human body; or two correct matching points are not the most similar in spectral domain. These stem from the limited constraints in low-dimensional functional space. To avoid this, we combine topological and functional spaces by constructing correspondences based on geometric LLE under relaxed spectral constraints (*i.e.*,  $K_2$  nearest neighbors). As shown in Fig. 2, the correspondence refinement via LLE can effectively reduce spectral ambiguity during an iterative

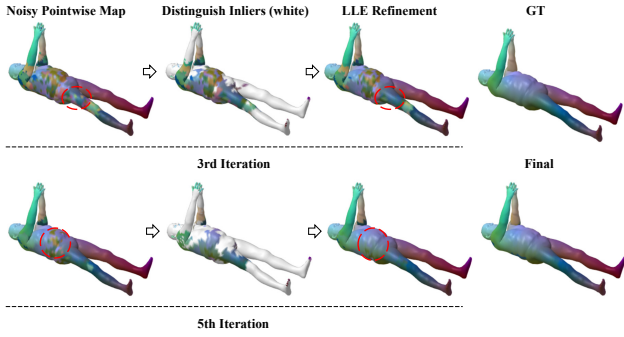


Figure 2: A visual illustration about the process of our LOPR, where LLE refinement for outliers after distinguishing inliers yields noticeable improvements.

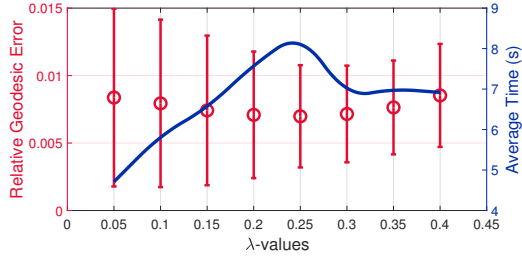


Figure 3: Parameter analysis of  $\lambda$ . Performance of LOPR under different  $\lambda$  values is evaluated using the mean and standard deviation of errors (Red), with the average time displayed on the right (Blue).

functional map framework. Additionally, for simple matching pair of shapes, we provide a cutoff condition to avoid redundant iterations, *i.e.*, the inlier set no longer grows, at which point the cardinality of inlier set can be regarded as a metric for evaluating the pointwise maps.

### Parameter Setting

Our method introduces three hyperparameters, *i.e.*,  $\lambda$ ,  $K_1$ ,  $K_2$ . We show how to set them in the following.

Parameter  $\lambda$  is the crucial threshold to determine the inlier set  $\mathcal{I}$ . To find an appropriate value, we select 200 shape pairs from the FAUST dataset (Bogo et al. 2014) as the test set, and use the whole LOPR for pointwise map recovery of MWP (Hu et al. 2021). Fig. 3 shows that  $\lambda$  can be set to 0.2 to balance the geometric errors and the runtime.

Parameter  $K_1$  determines the number of nearest neighbors in Eq. (14), which is used to construct local manifold representations in Eq. (15). Intuitively, a higher value of  $K_1$  is associated with stronger local geometric constraints but more time consumption. Considering a larger set  $\mathcal{I}$  can support more nearest neighbors for LLE, we empirically set an adaptive value for  $K_1$  *w.r.t.* the cardinality of  $\mathcal{I}$ , *e.g.*,  $K_1 = \lceil |\mathcal{I}|/100 \rceil$ , where  $\lceil \cdot \rceil$  means rounding up.

As in Eq. (17),  $K_2$  is the number of nearest neighbors searched in the spectral domain. As mentioned before, the larger the inlier set  $\mathcal{I}$  is, the more effective the local topological constraints preserved by matrix  $\mathbf{W}$  in Eq. (15), and consequently the larger the range over which suitable counterparts can be selected by Eq. (16). Therefore, it is proper

for  $K_2$  to be proportional to  $|\mathcal{I}|$ , *e.g.*,  $K_2 = \lceil |\mathcal{I}|/1000 \rceil$ .

Since  $\mathcal{I}$  is obtained by neighborhood consensus acting on initial pointwise map  $T_0$ , hence  $K_1$  and  $K_2$  are closely related to  $T_0$ . For a pair of shapes, the more accurate  $T_0$  is, the larger the inlier set  $|\mathcal{I}|$  is. Therefore, the larger values of  $K_1$  and  $K_2$  lead to more accurate pointwise map results but with higher computational cost.

### Computational Complexity

Our LOPR involves two main steps, namely inlier identification and correspondence refinement. In the first step, the computational cost is determined by the procedure of obtaining the disparity score  $c_i$  for each point. Given the adjacencies provided by the shape meshing, the computational complexity is  $O(N)$ , where  $N$  is the number of points on manifold  $\mathcal{M}$ .

The computational consumption of the second step depends on two K-nearest neighbor searches using K-D tree, and the complexities are  $O((K_1 + N_{\mathcal{O}}) \log N_{\mathcal{O}})$  and  $O((K_2 + N_{\mathcal{O}}) \log N_{\mathcal{O}})$ , where  $N_{\mathcal{O}}$  is the number of outliers on manifold  $\mathcal{M}$ . Since  $K_1 \ll N_{\mathcal{O}}$  and  $K_2 \ll N_{\mathcal{O}}$ , the time complexity of the second step can be simply written as  $O(N_{\mathcal{O}} \log N_{\mathcal{O}})$  and space complexity as  $O(N_{\mathcal{O}})$ .

Since  $N_{\mathcal{O}}$  and  $N$  belong to the same order of magnitude, therefore the proposed LOPR has linearithmic complexity for both time and space *w.r.t.* the number of points  $N$  on the manifold, which guarantees high efficiency of our method.

## Experiments

In this section, we apply our LOPR to challenging shapes from several public datasets and compare it with classical and state-of-the-art approaches.

### Implement Details

**Datasets** Four public datasets are used in our evaluation experiments:

- **FAUST** (Bogo et al. 2014) contains a total of 100 shapes, representing 10 poses of 10 different human subjects, exhibiting significant variations across different subjects. Each shape comprises 6890 element vertices, making it applicable even for computationally demanding methods. For quantitative evaluation, we randomly selected 300 shape pairs, encompassing both isometric and non-isometric deformations.
- **TOSCA** (Bronstein, Bronstein, and Kimmel 2008) provides 76 shapes divided into 8 distinct categories (ranging from human to animal), with almost every shape containing 10k vertices. Our experimental evaluation involves all isometric shape pairs, totaling 414 pairs.
- **SCAPE** (Anguelov et al. 2005) contains 71 registered meshes representing different poses of the same human subject. Each of these meshes consists of 12500 vertices. We randomly selected 200 matching pairs for quantitative evaluations.
- **TOPKIDS** (Löhner et al. 2016) consists of 26 non-intersecting manifold shapes, which are generated by merging self-intersecting parts of the shapes from KIDS

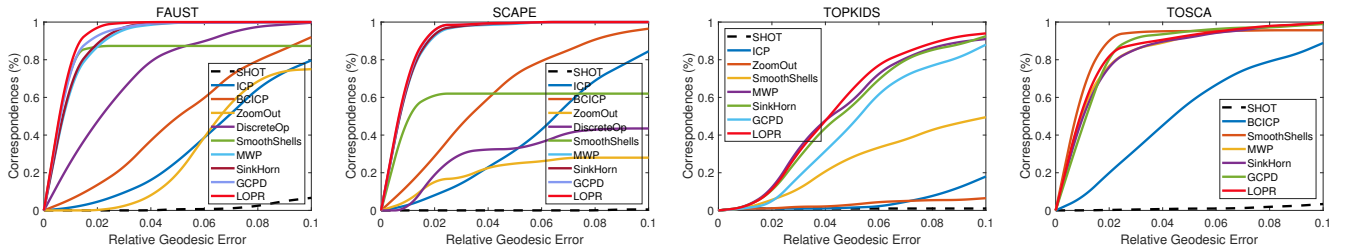


Figure 4: Evaluations of our LOPR with other methods on FAUST, SCAPE, TOPKIDS, and TOSCA datasets with CQCs.

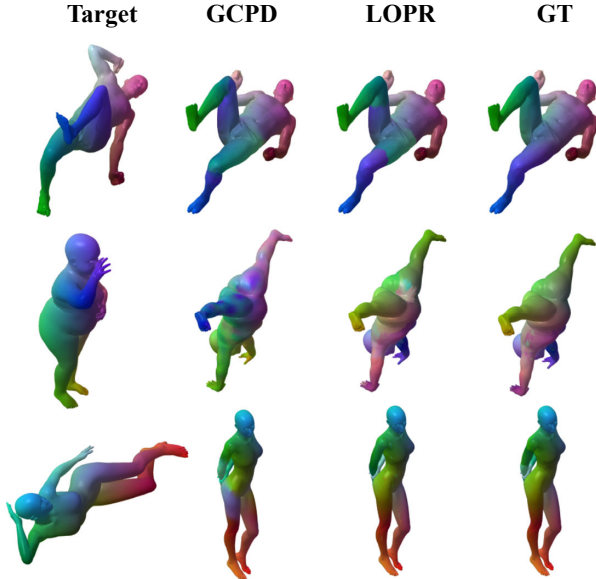


Figure 5: Qualitative demonstration using color transfer. In each row of results, the first and last shapes represent the target and source shapes matched with the ground truth respectively, the second shape depicts the result of GCPD, while the third shape represents the result of our LOPR. The shapes in the topmost row originate from SCAPE, those in the second row are sourced from TOPKIDS, and the ones in the bottom row are from TOSCA.

dataset (Rodola et al. 2014) thus highly challenging. We randomly selected 200 matching pairs from low-resolution shapes (each mesh contains approximately 10k vertices) for quantitative evaluations.

**Evaluation** Princeton benchmark protocol (Kim, Lipman, and Funkhouser 2011) is used to evaluate the accuracy of shape matching. Specifically, given a ground-truth correspondence  $(\mathbf{x}, \mathbf{y}^*)$  where  $\mathbf{x} \in \mathcal{X}$  and  $\mathbf{y}^* \in \mathcal{Y}$ , the error for obtained correspondence  $(\mathbf{x}, \mathbf{y})$  is calculated by relative geodesic distance between  $\mathbf{y}$  and  $\mathbf{y}^*$  normalized by diameter of  $\mathcal{Y}$ :  $\epsilon(x) = \frac{d_{\text{geo}}(\mathbf{y}, \mathbf{y}^*)}{\sqrt{\text{area}(\mathcal{Y})}}$ . We employ the Correspondence Quality Characteristics (CQC) curves (Kim, Lipman, and Funkhouser 2011), which depict the percentages of matches that have geodesic errors no greater than  $r$ , and the average geodesic error across all vertices on the shape  $\mathcal{M}$ , to quantify the correspondence quality.

**Competitors** The competitor methods include ICP (Ovsjanikov et al. 2012), BCICP (Ren et al. 2018),

Methods	FAUST	SCAPE	TOPKIDS	TOSCA
SmoothShells	0.0442	0.1175	0.1625	0.0198
MWP	0.0100	0.0096	0.0502	0.0171
Sinkhorn	0.0089	0.0096	0.0515	0.0175
GCPD	0.0084	<b>0.0087</b>	0.0709	0.0159
LOPR	<b>0.0070</b>	0.0091	<b>0.0466</b>	<b>0.0157</b>

Table 1: Average relative geodesic errors of our LOPR and state-of-the-arts on four public datasets, where the **bold** indicates the best.

ZoomOut (Melzi et al. 2019), DiscreteOp (Ren et al. 2021), SmoothShells (Eisenberger, Lahner, and Cremers 2020), MWP (Hu et al. 2021), Sinkhorn (Pai et al. 2021), and GCPD (Fan et al. 2022).

**Settings** The matching results in SHOT (Tombari, Salti, and Di Stefano 2010) descriptor space are used as initialization for ICP, BCICP, DiscreteOp, and MWP. GCPD uses the results of MWP as the input. Sinkhorn and our LOPR are used to recover pointwise maps of MWP with 5 discrete filters and 4 iterations. For all competitors, we use the settings and codes provided online by their authors. In particular, the number of eigenfunctions is uniformly set to 500, which for ZoomOut is the maximal dimension of its upsampling iterations. As suggested by its authors, GCPD is initialized by MWP with 200 eigenfunctions, and the subsequent smoothing model is still based on a 500-dimensional eigenfunction space. All experiments are conducted on a PC with Intel(R) Core i9-9920X CPU at 3.50GHz, using MATLAB R2018a. And  $K$ -nearest neighbor search is accelerated by GPU.

## Results Analysis

The quantitative evaluations on four public datasets include CQC curves and average errors, which are shown in Fig. 4 and Table 1, respectively. MWP (Hu et al. 2021), Sinkhorn (Pai et al. 2021), and GCPD (Fan et al. 2022), as the recent State-Of-The-Art (SOTA) methodologies, exhibit evident advantages over their predecessors, notably demonstrated on the FAUST, SCAPE, and TOPKIDS datasets. Notably, GCPD, as a SOTA advancement, employs MWP to initialize an externally-deformation-based probabilistic model and demonstrates decent performances. However, our method consistently achieves lower average errors across the majority of datasets, as illustrated in Table 1. Qualitative comparisons between our LOPR and GCPD are provided in Fig. 5, where the second row comes from the TOPKIDS dataset (see the third sub-figure in Fig. 4 for quantitative

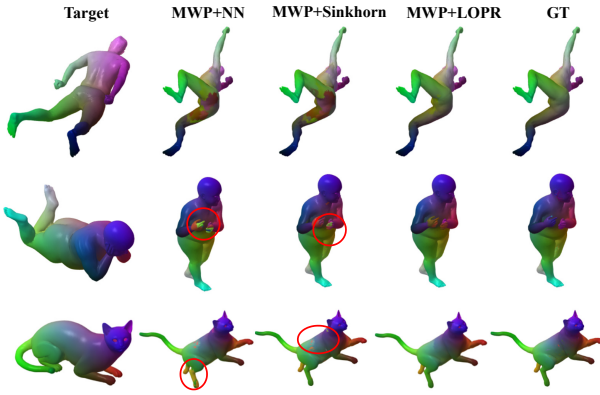


Figure 6: Qualitative comparisons for NN, Sinkhorn, and our LOPR on MWP using color transfer. The shapes in the top-most row originate from SCAPE, those in the second row are sourced from TOPKIDS, and the ones in the bottom row are from TOSCA. Best viewed zoomed in.

Methods	FAUST	SCAPE	TOPKIDS	Wolf	Michael
#Vertices	6890	12500	10399	4344	10000
SmoothShells	98.957	161.03	113.68	56.979	112.54
MWP	1.8358	4.3591	3.6495	0.8974	3.1439
GCPD	9.3658	20.146	14.184	2.8385	12.615
Sinkhorn	24.072	101.70	63.872	10.010	64.415
LOPR	3.9523	13.357	9.4687	1.4258	7.1651

Table 2: Average runtime (in seconds) demonstration of our LOPR and state-of-the-art on different resolutions. We present the results on FAUST, SCAPE, and TOPKIDS datasets and two models (Wolf and Michael) of TOSCA.

analysis). These visual comparisons underscore LOPR’s superior capability to address intricate matching pairs, exemplified by challenging datasets such as TOPKIDS.

In addressing the pointwise map recovery problem, analogous methods include classical Nearest Neighbors (NN) (Ovsjanikov et al. 2012) and the recent Sinkhorn (Pai et al. 2021) method. To visually contrast our method with these competitors, qualitative comparisons are showcased in Fig. 6. Here, the functional map matrices are uniformly computed utilizing MWP with 5 iterations. Evidently, our LOPR excels in recovering more accurate pointwise correspondences comparing classic NN and representative Sinkhorn, which is due to that both of them lack the geometric constraints of the external space.

Furthermore, the average runtimes of our method, alongside several representative techniques, are reported in Table 2. The runtime of our LOPR is deemed acceptable across various shape resolutions, notably outpacing the recent methods Sinkhorn and GCPD due to the linearithmic computational complexity of our LOPR.

## Partial Matching

The geometric constraints embedded in LOPR are rooted in the consistency of small local regions during deformation, displaying broad applicability, even in partial matching.

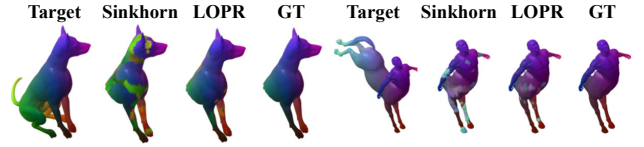


Figure 7: Qualitative examples of our LOPR and Sinkhorn on partial shape matching using color transfer. In each of these two groups, the first and last shapes are target and source shapes with ground-truth matching, the second shape is the result of Sinkhorn, and the third shape represents the results of our LOPR.

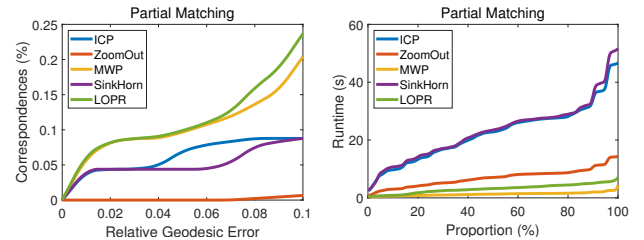


Figure 8: Quantitative comparisons for our LOPR and state-of-the-art functional map methods on partial shape matching tasks. The left contains the CQC curve of each method, while the right shows the cumulative distribution function of runtime, where the point situated along the curve at coordinates  $(x, y)$  signifies that the runtime does not exceed  $y$  for a percentage of  $x\%$  of the instances.

Employing the cuts dataset provided by Partial Functional Correspondences (Rodolà et al. 2017), which encompasses 456 partial shapes spanning different classes of TOSCA, we compare our LOPR with representative functional map methods to achieve partial-to-full matching. Qualitative instances of comparing our LOPR with SOTA Sinkhorn are presented in Fig. 7, where our LOPR can achieve more accurate and continuous pointwise maps, attributed to the weaker generality of optimal transport modeling of Sinkhorn. From quantitative CQC curves and runtime results illustrated in Fig. 8, comparing with other functional map methods, our method is capable of achieving competitive accuracy improvements within a moderate time cost.

## Conclusion

In this paper, we propose a concise and efficient framework for pointwise map recovery in functional maps to address nonrigid shape matching, named *LOcality Preserving Refinement* (LOPR). The geometric constraints we apply are based on local consistency, wherein small regions on a manifold exhibit invariance across various deformations, including nonrigid transformation. The process of LOPR involves two steps, *i.e.*, outlier identification based on neighborhood support and correspondence refinement via LLE. Neighborhood support enforces continuity among points within local regions, while the utilization of LLE eliminates spectral ambiguities such as intrinsic symmetries. Experimental results on four benchmarks validate the superiority of our LOPR over the state-of-the-art in terms of accuracy. Moreover, partial matching experiments underscore the generality of LOPR for intricate deformations.

## Acknowledgments

This work was supported by the National Natural Science Foundation of China (62276192).

## References

- Anguelov, D.; Srinivasan, P.; Koller, D.; Thrun, S.; Rodgers, J.; and Davis, J. 2005. SCAPE: shape completion and animation of people. *ACM Transactions on Graphics (TOG)*, 24(3): 408–416.
- Bogo, F.; Romero, J.; Loper, M.; and Black, M. J. 2014. FAUST: Dataset and evaluation for 3D mesh registration. In *Proceedings of the IEEE Conference on Computer Vision and Pattern Recognition*, 3794–3801.
- Bronstein, A. M.; Bronstein, M. M.; and Kimmel, R. 2008. *Numerical geometry of non-rigid shapes*. Springer Science & Business Media.
- Deng, B.; Yao, Y.; Dyke, R. M.; and Zhang, J. 2022. A Survey of Non-Rigid 3D Registration. *Computer Graphics Forum*, 41(2): 559–589.
- Donati, N.; Corman, E.; Melzi, S.; and Ovsjanikov, M. 2022. Complex functional maps: A conformal link between tangent bundles. *Computer Graphics Forum*, 41(1): 317–334.
- Eisenberger, M.; Lahner, Z.; and Cremers, D. 2020. Smooth shells: Multi-scale shape registration with functional maps. In *Proceedings of the IEEE Conference on Computer Vision and Pattern Recognition*, 12265–12274.
- Ezuz, D.; and Ben-Chen, M. 2017. Deblurring and denoising of maps between shapes. *Computer Graphics Forum*, 36(5): 165–174.
- Fan, A.; Ma, J.; Tian, X.; Mei, X.; and Liu, W. 2022. Coherent Point Drift Revisited for Non-rigid Shape Matching and Registration. In *Proceedings of the IEEE Conference on Computer Vision and Pattern Recognition*, 1424–1434.
- Hartman, E.; Sukurdeep, Y.; Klassen, E.; Charon, N.; and Bauer, M. 2023. Elastic shape analysis of surfaces with second-order sobolev metrics: a comprehensive numerical framework. *International Journal of Computer Vision*, 131(5): 1183–1209.
- Hu, L.; Li, Q.; Liu, S.; and Liu, X. 2021. Efficient deformable shape correspondence via multiscale spectral manifold wavelets preservation. In *Proceedings of the IEEE Conference on Computer Vision and Pattern Recognition*, 14536–14545.
- Jiang, L.; Lee, C.; Teotia, D.; and Ostadabbas, S. 2022. Animal pose estimation: A closer look at the state-of-the-art, existing gaps and opportunities. *Computer Vision and Image Understanding*, 103483.
- Kim, V. G.; Lipman, Y.; and Funkhouser, T. 2011. Blended intrinsic maps. *ACM Transactions on Graphics*, 30(4): 1–12.
- Löhner, Z.; Rodolà, E.; Bronstein, M. M.; Cremers, D.; Burghard, O.; Cosmo, L.; Dieckmann, A.; Klein, R.; Sahillioğlu, Y.; et al. 2016. SHREC’16: Matching of deformable shapes with topological noise. In *Proceedings of the Eurographics Workshop on 3D Object Retrieval*, 55–60.
- Magnet, R.; Ren, J.; Sorkine-Hornung, O.; and Ovsjanikov, M. 2022. Smooth non-rigid shape matching via effective Dirichlet energy optimization. In *Proceedings of the International Conference on 3D Vision*, 495–504.
- Melzi, S.; Ren, J.; Rodola, E.; Sharma, A.; Wonka, P.; and Ovsjanikov, M. 2019. Zoomout: Spectral upsampling for efficient shape correspondence. *arXiv preprint arXiv:1904.07865*.
- Myronenko, A.; and Song, X. 2010. Point set registration: Coherent point drift. *IEEE Transactions on Pattern Analysis and Machine Intelligence*, 32(12): 2262–2275.
- Ovsjanikov, M.; Ben-Chen, M.; Solomon, J.; Butscher, A.; and Guibas, L. 2012. Functional maps: a flexible representation of maps between shapes. *ACM Transactions on Graphics*, 31(4): 1–11.
- Ovsjanikov, M.; Corman, E.; Bronstein, M.; Rodolà, E.; Ben-Chen, M.; Guibas, L.; Chazal, F.; and Bronstein, A. 2016. Computing and processing correspondences with functional maps. In *SIGGRAPH ASIA 2016 Courses*, 1–60.
- Pai, G.; Ren, J.; Melzi, S.; Wonka, P.; and Ovsjanikov, M. 2021. Fast sinkhorn filters: Using matrix scaling for non-rigid shape correspondence with functional maps. In *Proceedings of the IEEE Conference on Computer Vision and Pattern Recognition*, 384–393.
- Penney, R. 1975. Abstract Plancherel theorems and a Frobenius reciprocity theorem. *Journal of Functional Analysis*, 18(2): 177–190.
- Ren, J.; Melzi, S.; Wonka, P.; and Ovsjanikov, M. 2021. Discrete optimization for shape matching. *Computer Graphics Forum*, 40(5): 81–96.
- Ren, J.; Poulenard, A.; Wonka, P.; and Ovsjanikov, M. 2018. Continuous and orientation-preserving correspondences via functional maps. *ACM Transactions on Graphics*, 37(6): 1–16.
- Rodolà, E.; Cosmo, L.; Bronstein, M. M.; Torsello, A.; and Cremers, D. 2017. Partial functional correspondence. *Computer Graphics Forum*, 36(1): 222–236.
- Rodolà, E.; Moeller, M.; and Cremers, D. 2015. Point-wise map recovery and refinement from functional correspondence. *arXiv preprint arXiv:1506.05603*.
- Rodola, E.; Möller, M.; and Cremers, D. 2017. Regularized pointwise map recovery from functional correspondence. *Computer Graphics Forum*, 36(8): 700–711.
- Rodola, E.; Rota Bulò, S.; Windheuser, T.; Vestner, M.; and Cremers, D. 2014. Dense non-rigid shape correspondence using random forests. In *Proceedings of the IEEE Conference on Computer Vision and Pattern Recognition*, 4177–4184.
- Roetzer, P.; Swoboda, P.; Cremers, D.; and Bernard, F. 2022. A scalable combinatorial solver for elastic geometrically consistent 3d shape matching. In *Proceedings of the IEEE Conference on Computer Vision and Pattern Recognition*, 428–438.
- Roweis, S. T.; and Saul, L. K. 2000. Nonlinear dimensionality reduction by locally linear embedding. *Science*, 290(5500): 2323–2326.

- Sahillioglu, Y. 2020. Recent advances in shape correspondence. *The Visual Computer*, 36(8): 1705–1721.
- Sumner, R. W.; and Popović, J. 2004. Deformation transfer for triangle meshes. *ACM Transactions on Graphics*, 23(3): 399–405.
- Tombari, F.; Salti, S.; and Di Stefano, L. 2010. Unique signatures of histograms for local surface description. In *Proceedings of the European Conference on Computer Vision*, 356–369.
- Van Kaick, O.; Zhang, H.; Hamarneh, G.; and Cohen-Or, D. 2011. A survey on shape correspondence. *Computer Graphics Forum*, 30(6): 1681–1707.
- Vestner, M.; Löhner, Z.; Boyarski, A.; Litany, O.; Slossberg, R.; Remez, T.; Rodola, E.; Bronstein, A.; Bronstein, M.; Kimmel, R.; et al. 2017a. Efficient deformable shape correspondence via kernel matching. In *Proceedings of the International Conference on 3D Vision*, 517–526.
- Vestner, M.; Litman, R.; Rodola, E.; Bronstein, A.; and Cremers, D. 2017b. Product manifold filter: Non-rigid shape correspondence via kernel density estimation in the product space. In *Proceedings of the IEEE Conference on Computer Vision and Pattern Recognition*, 3327–3336.